Electronic Supplementary Information

Multi floor Cascading Ferroelectric Nanostructures: Multiple Data Writing-Based Multi-level Non-Volatile Memory Devices

Seung Hyun[a+], Owoong Kwon[b+], Bom-yi Lee[a], Daehee Seol[b], Beomjin Park[a], Jae Yong Lee[a], Ju Hyun Lee[a], Yunseok Kim[b], Jin Kon Kim[a]**

[a]National Creative Research Initiative Center for Smart Block Copolymer Self-Assembly, Department of Chemical Engineering, Pohang University of Science and Technology (POSTECH), Pohang, Gyungbuk 790-784, Republic of Korea

E-mail: jkkim@postech.ac.kr

[b]School of Advanced Materials Science and Engineering, Sungkyunkwan University, Suwon, Gyeonggi-do 440-746, Republic of Korea

E-mail: yunseokkim@skku.edu

S1. Fabrication of AAO template with inverse multi floor cascading pores

Anodic aluminum oxide (AAO) membrane was prepared as follows. A highly pure aluminum plate (99.999 %, 1 mm thickness) was sonicated in acetone for 30 min and electrochemically polished twice in a polishing solution (ethanol: perchloric acid ($HClO_4$) = 4 : 1 v/v) at 7 °C and 20 V for 30 min. Polished aluminum plate was washed with ethanol and deionized water alternately. The anodization was carried out with 0.1 M phosphoric acid (H_3PO_4) aqueous solution at 0 °C and 195 V for 12 h, and was etched by an etchant solution (1.8 wt % chromic acid (H_2CrO_4) and 6 wt % H_3PO_4 in deionized (DI) water) at 65 ^oC for over 5 h, and washed by DI water.

The first step of the fabrication on multi floor cascading pores was achieved by anodizing aluminum with 0.1 M H_3PO_4 aqueous solution at 0 °C and 195 V for 90 s, generating hexagonally packed cylindrical nanopores of a diameter (D) of 100 nm and a thickness (H) of 200 nm, as shown in top and cross-sectional SEM images given in Figs. S1a1 and S1b1. Those pores were enlarged after the first etching step by the immersion of the sample in 0.1 M H_3PO_4 aqueous solution at 30 °C for 150 min, producing D = 250 nm and H = 200 nm, as shown in Figs. S1a2 and S1b2. During the etching process, because the whole surface of AAO template is etched, D is only enlarged, but H does not change.

When the second step of anodization was performed, smaller pores were newly generated below the pores obtained after the first etching step, which produces inverse cascading two floor pores. Namely, the size (D = 250 nm and H = 200 nm) of the upper pores referred as to “the first floor” pores are the same as those obtained after the first etching step. The smaller pores (D = 100 nm and H = 200 nm) are generated at the lower parts of the AAO template, which is referred to as “the second floor” (See Figs. S1a3 and S1b3). After the second etching

process, the pore diameters in both floors are enlarged. The pores in the first floor have D = 400 nm and H = 200 nm, while those in the second floor have D = 250 nm and H = 200 nm, as shown in Figs. S1a4 and S1b4. This pore structures after the second etching process are referred to as “inverse two floor cascading pores”.

To make “inverse three floor cascading pores”, we performed one more anodization. The size of pores in each floor is as follows: (1) pores in the first floor have D = 400 nm and H = 200 nm, (2) pores in the second floor have D = 250 nm and H = 200 nm, and (3) pores in the third floor have D = 100 nm and H = 200 nm, as shown in Figs. S1a5 and S1b5.

Furthermore, H in the AAO templates is easily controlled by anodization time. For instance, H increased with anodization time at a rate of 133 nm/min, as shown in Fig. S1c, when anodization was performed at 0.1 M H_3PO_4 aqueous solution at 0 °C and 195 V. Fig. S1d shows that D in the AAO templates increased with etching time at a rate of 1 nm/min under 0.1 M H_3PO_4 aqueous solution at 30 °C. Thus, one can in principle fabricate AAO templates with inverse multi floor cascading pores with various D and H by controlling anodization and etching times, respectively.

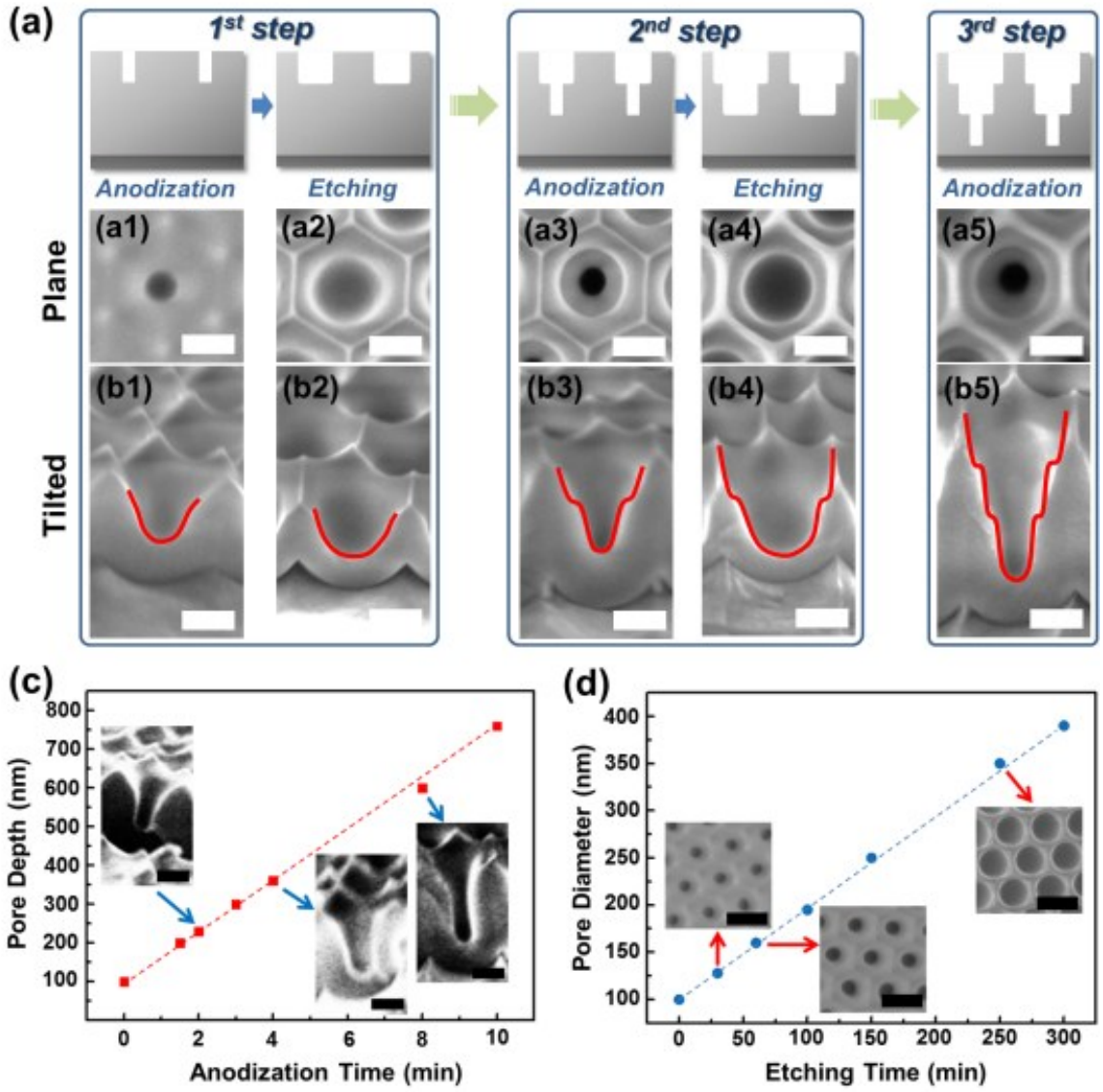

Fig. S1. Fabrication of AAO template with inverse multi floor cascading pores by repeated anodization and etching processes by H_3PO_4 aqueous solution. Top panel gives a schematic of each process. (a1-a5) and (b1-b5) give top views and 90 ° tilted views of SEM images corresponding to each step, respectively. Scale bar is 200 nm. (c) The change of pore depth (*H*) with anodization time under 0.1 M H_3PO_4 aqueous solution at 0 °C and 195 V. Scale bar is 200 nm. (d) The variation of pore diameter (*D*) with etching time under 0.1 M H_3PO_4 aqueous solution at 30 °C. Scale bar is 500 nm.

S2. Chemical cross-linking reaction between P(VDF-TrFE) and THDA

We used 2,4,4-trimethyl-1,6-hexanediamine (THDA) as a cross-linking agent. Due to the electrodonating groups (methyl (R-CH_3) and neopentyl (R-C_3H_9)), THDA allows dehydrofluorination of P(VDF-TrFE) and forms a double bond between carbon of P(VDF-TrFE) main chain and nitrogen of THDA by thermal annealing, producing chemical bridge between C and N, as shown in Fig. S2.

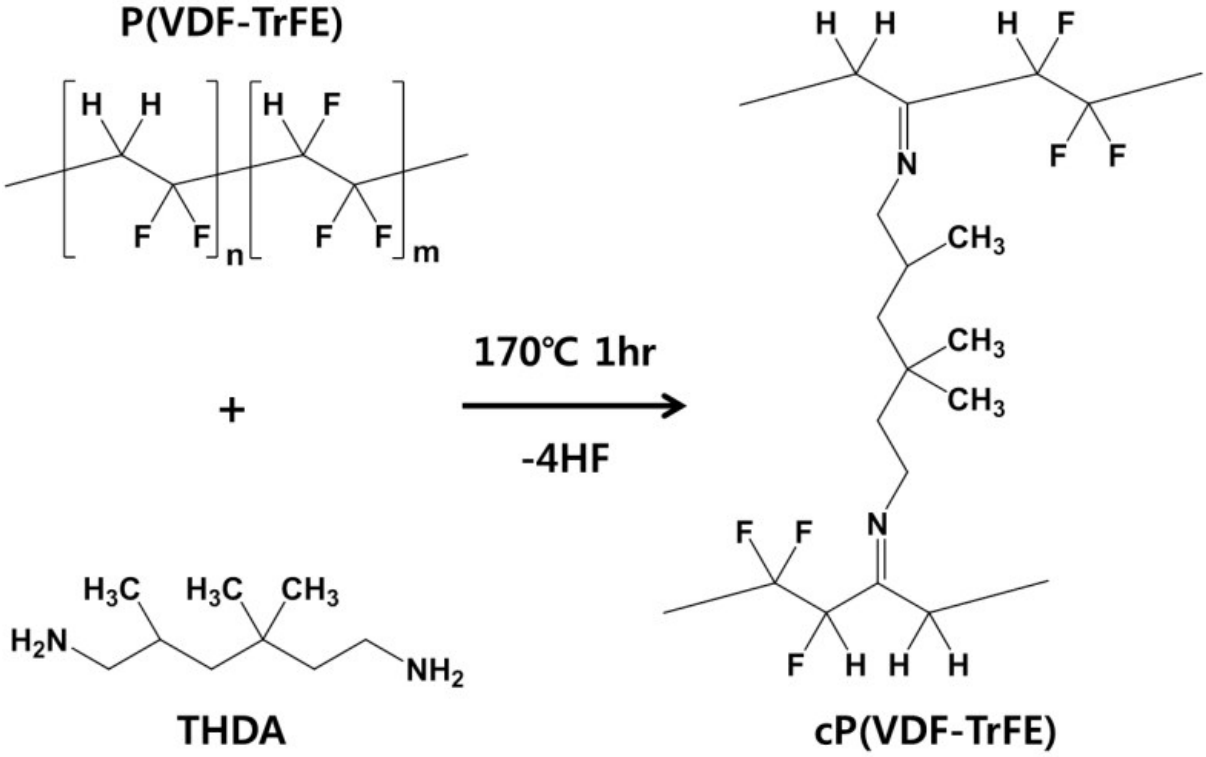

Fig. S2. Chemical reaction between P(VDF-TrFE) and THDA at high temperature.

S3. XPS data for identifying chemical cross-linking reaction between P(VDF-TrFE) and THDA

To confirm the formation of imine bond (C=N), we performed X-ray photoelectron spectroscopy (XPS). Figs. S3a and S3b show C 1s and N 1s XPS spectra, respectively, of P(VDF-TrFE) with 10 wt % of THDA. The background and peaks in Fig. S3a were obtained by fitting using Shirley background mode and Gaussian mode, respectively. The peaks at 286.7 eV and 398.5 eV are clearly seen, corresponding to C 1s and N 1s in C=N bonds (See Table S1). This indicates that P(VDF-TrFE) chains were successfully linked by THDA to form C=N linkage.

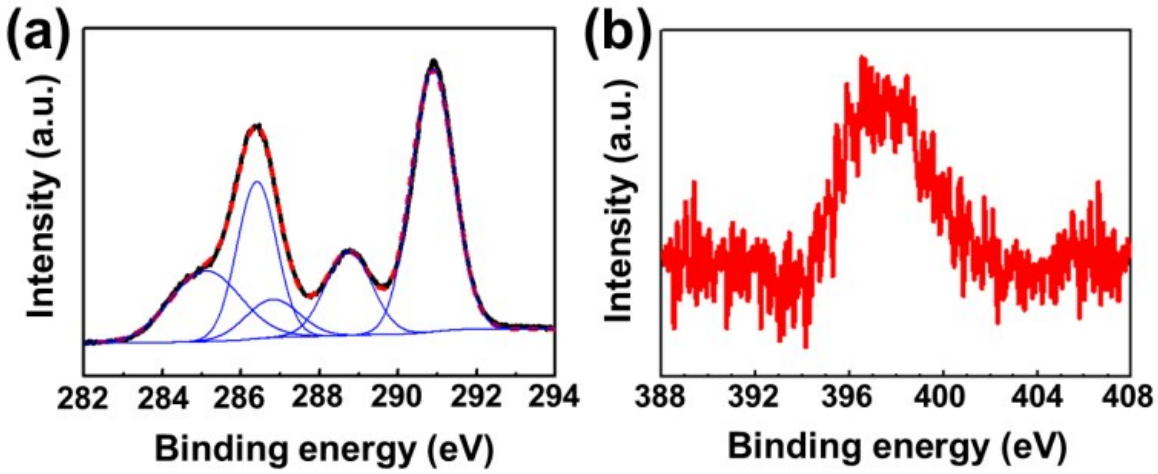

Fig. S3. XPS spectra of (a) C 1s and (b) N 1s for P(VDF-TrFE) with 10 wt % of THDA. The background and the deconvoluted peaks in C 1s spectrum were obtained by fitting using Shirley background mode and Gaussian mode, respectively

Table S1 Binding energy of C 1s and N 1s in various bonds.

Type	Bond	Binding energy (eV)
C 1s	C-C, C-H, C-N	285
	CH_2	286.4
	C=N	286.7
	$-CF_2-CF_2-$	289.3
	$-CF_2-CFH-$	291.1
N 1s	-N=C-	398.5

S4. High performance on chemical stability and leakage current of cross-linked P(VDF-TrFE)

Cross-linked P(VDF-TrFE) shows the excellent solvent resistance, as shown in Fig. S5. When the sample was exposed to acetone vapor for 1 h, the cross-linked P(VDF-TrFE) nanostructures maintained their original shape, while uncross-linked (neat) P(VDF-TrFE) nanostructures was severely collapsed (Figs. S4a and S4b).

The most important aspect of the cross-linked P(VDF-TrFE) is to minimize leakage current. Because a leakage current induces undesirable polarization switching of ferroelectric domain and loss of storage information, the maintenance of negligible leakage current is very important for the ferroelectric based memory devices. Fig. S4c shows the leakage current density versus voltage depending on the existence of THDA. Very large leakage current of a sample without THDA was dramatically suppressed (~order of 10^5) by the addition of 10 wt % of THDA to P(VDF-TrFE), which means that the cross-linking effectively prevents the tunneling current.

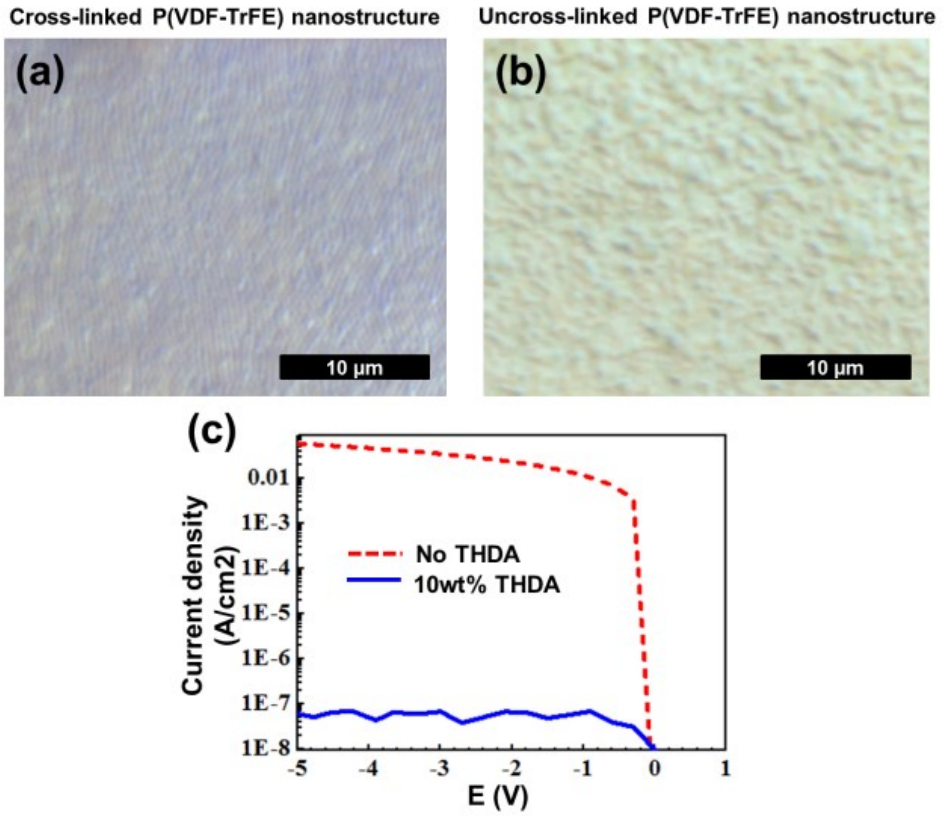

Fig. S4. OM images of (a) cross-linked and (b) uncross-linked P(VDF-TrFE) nanostructures after the samples were exposed to saturated acetone vapor for 1 h at room temperature. (c) Leakage current density of P(VDF-TrFE) without (dotted line) and with (solid line) 10 wt % of THDA.

S5. Size distribution of cP(VDF-TrFE) nanostructures

From the AFM topography images of the two and three floor cP(VDF-TrFE) nanostructures, we measured the size distribution of the diameter (D) and height (H) as shown in Fig. S5. The dimensions of the cP(VDF-TrFE) nanostructures in each floor of the two floor geometry are (1) D = 400 ± 5 nm and H = 200 ± 4 nm for the first floor and (2) D = 250 ± 3 nm and H = 200 ± 4 nm for the second floor, respectively. In the case of three floor nanostructures, the dimensions of the additional third floor show D = 100 ± 1 nm and H = 200 ± 3 nm, respectively. The size of each floor of the cP(VDF-TrFE) nanostructure is nearly the same as that of inverse multi floor cascading pores in the AAO template.

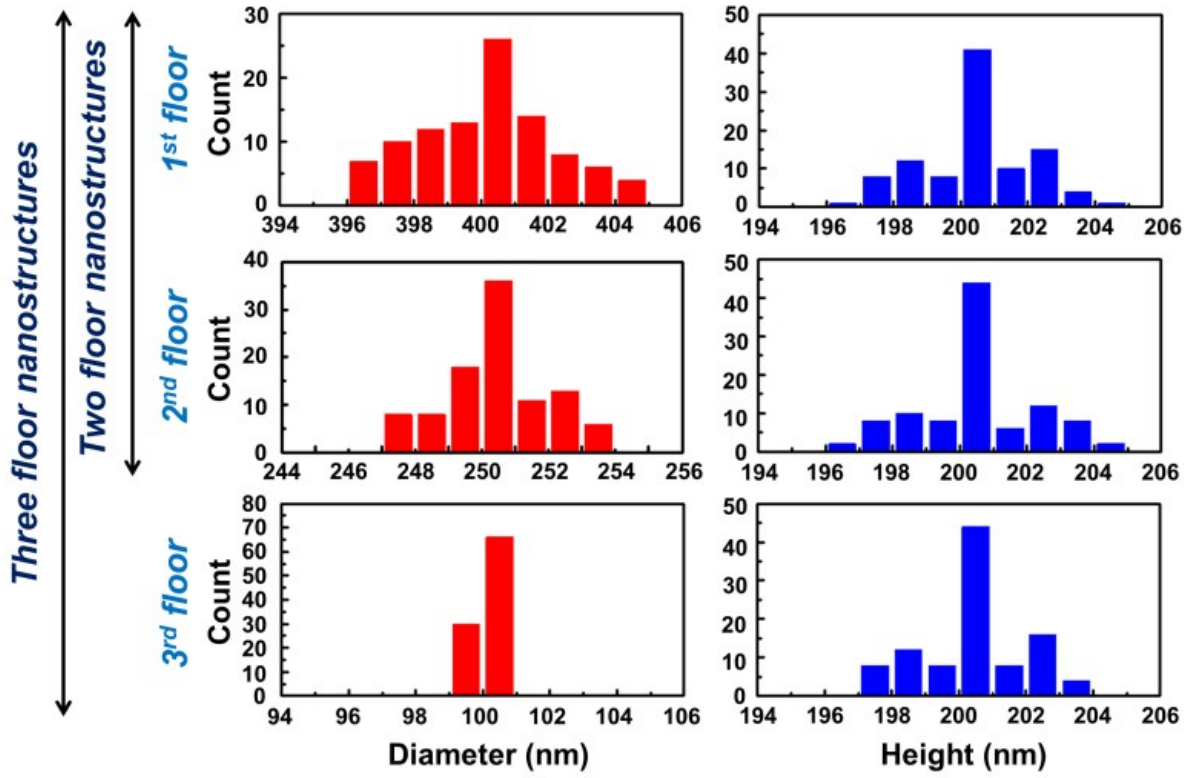

Fig. S5. Diameter and height distribution of each floor of two and three floor cascading cP(VDF-TrFE) nanostructures.

S6. Chain conformation of cP(VDF-TrFE) nanostructure and continuous film

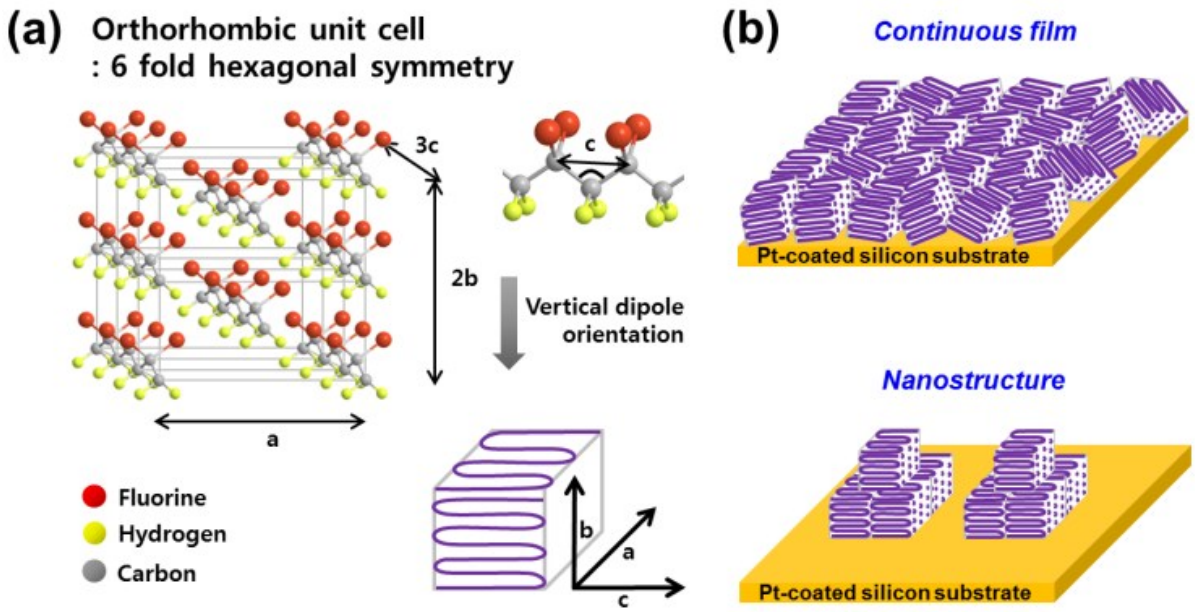

Fig. S6. (a) Orientation of crystal unit of P(VDF-TrFE) with a vertical polar *b* axis and in-plane *a* and *c* axes. (b) Schematic illustration showing chain orientation of P(VDF-TrFE) in continuous film and nanostructures on Pt-coated silicon substrate.

S7. SS-PFM images of c(PVDF-TrFE) nanostructures

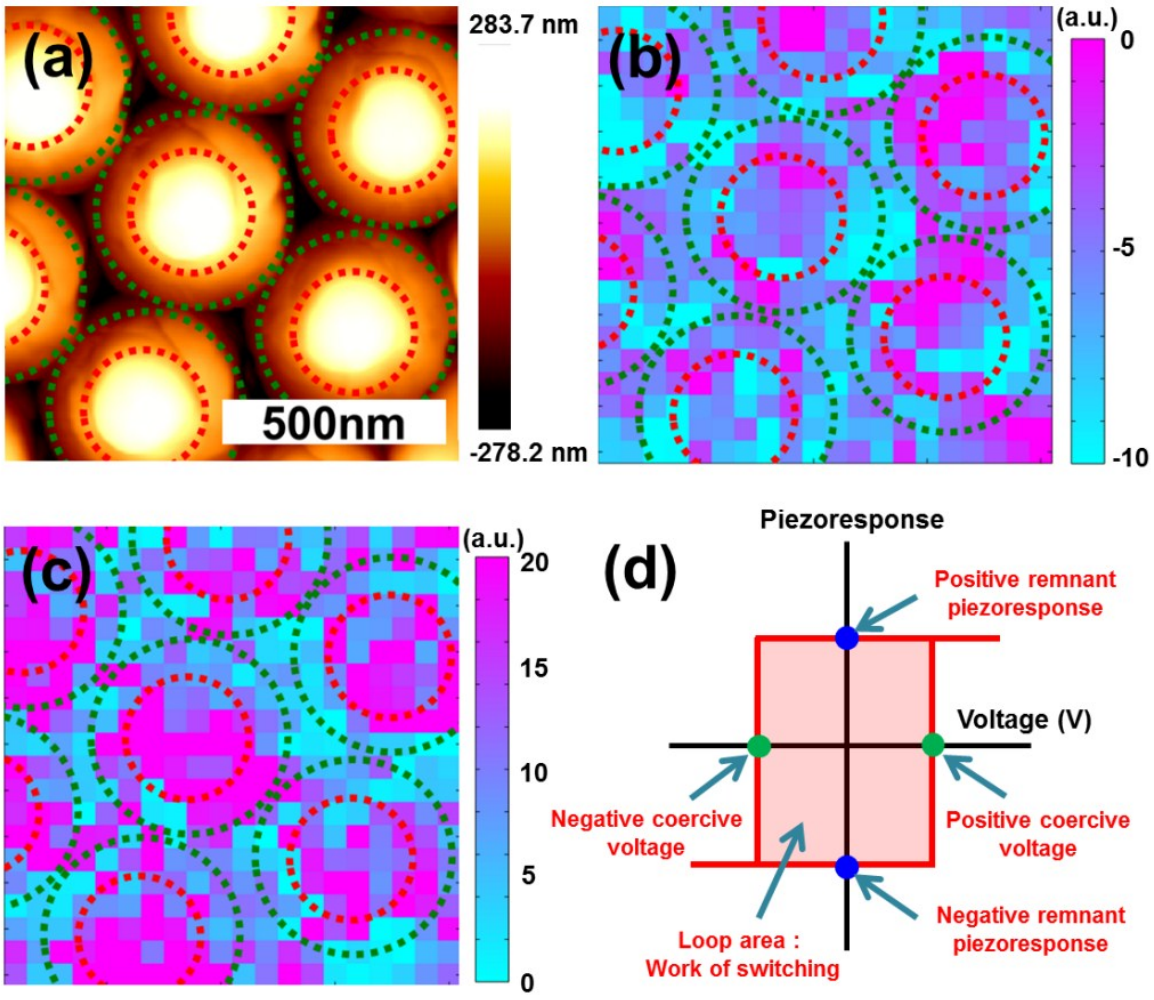

Fig. S7. (a) Topology of two floor cascading cPVDF nanostructures and corresponding spatial maps of (b) negative remnant piezoresponse and (c) work of switching. (d) The physical meaning of the nomenclatures used in the main text.

S8. Discussion about the size and aspect ratio of the tip relative to the size and shape of the two floor cP(VDF-TrFE) nanostructure for measuring piezoresponse

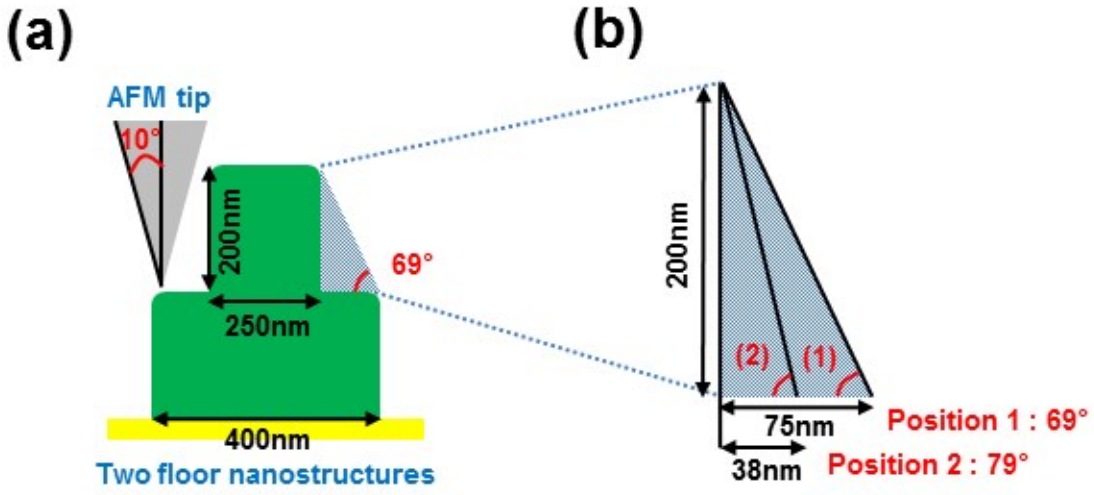

Fig. S8. Schematics of (a) AFM tip and two floor c(PVDF-TrFE) nanostructure and (b) angles between the first and second floor depending on the position on the first floor.